Coupling of two resonant modes for insect wing mimicking in a flexible-wing NAV and generate lift

Damien Faux, Eric Cattan, Sébastien Grondel, Olivier Thomas

COUPLING OF TWO RESONANT MODES FOR INSECT WING MIMICKING IN A FLEXIBLE-WING NAV AND GENERATE LIFT

Damien Faux *, Eric Cattan, Sebastien Grondel
Univ. Valenciennes, CNRS, Univ. Lille, YNCREA, Centrale Lille
UMR 8520 - IEMN, DOAE
F-59313 Valenciennes
France
damien.faux@univ-valenciennes.fr *
eric.cattan@univ-valenciennes.fr
sebastien.grondel@univ-valenciennes.fr

Olivier Thomas
Arts et Métiers ParisTech
LSIS
8 boulevard Louis XIV 59046 Lille
France
olivier.thomas@ensam.eu

ABSTRACT

This work is based on the original concept of coupling two resonant vibration modes to reproduce insect wing kinematics and generate lift. The key issue is designing the geometry and the elastic properties of the artificial wings to achieve quadrature coupling of the bending and twisting motions using only one actuator. Qualitatively, this implies bringing the frequency of the two resonant modes closer. In the light of this challenge, an optimal wing configuration was determined for a micromachined polymer prototype three centimeters wide and validated through experimental modal analyses to illustrate the proximity of the frequencies of the bending and twisting modes. Then, a dedicated lift force measurement bench was developed and used to demonstrate a lift force equivalent to 110% of the prototype weight. For the first time, high-speed camera measurements of the wing motion confirmed that maximum lift was obtained as expected for bending and twisting motions in phase quadrature with a fully resonant motion of the wings using a single actuator.

* Address all correspondence to this author.

1 Introduction

Among flying species observed in nature, insects certainly demonstrate the most impressive capacities in terms of hovering, backward flight or sudden acceleration, and their diversity offers multiple solutions for bioinspired systems. Understanding of insect flight has improved considerably, and it is well known that lift results from a wide array of unconventional aerodynamic mechanisms [1] as well as specific kinematics induced by the flexible characteristics of the wings [2], and more precisely, as illustrated in Fig. 1 through the generic periodic motion of the wing cross section in the chord direction. Insect wing motion relies on the combination of four basic motions: the downstroke, supination, the upstroke, and pronation [3, 4].

In the case of flexible wings, the up and downstrokes involve a bending motion whereas supination and pronation result in a twisting motion in quadrature with the previous motion. This phase quadrature, i.e. when the amplitude is maximal for one motion it is null for the other, produces aerodynamic forces and contributes to generating lift. As already mentioned, a key element of insect flight is the flexibility of the wing structure that often changes shape dynamically during flight [7], but its exact role in aerodynamic performance remains unclear and controversial. Several studies [2, 8, 9] have provided direct evidence that flexible wings that can produce camber generate higher peak lift forces than rigid wings [10, 11], but recent simulations [12]

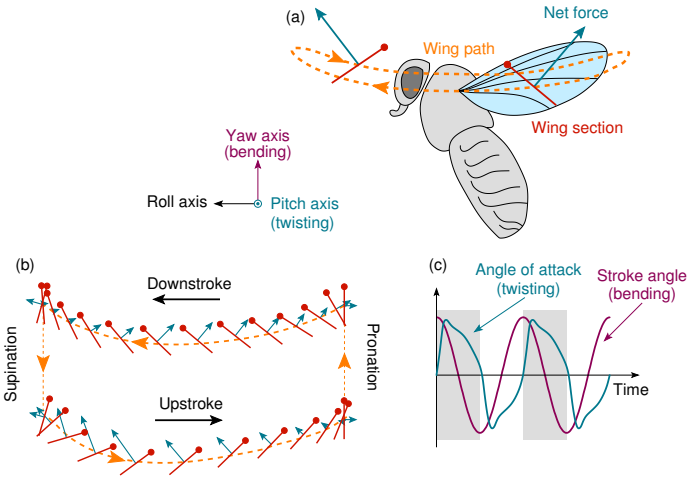

FIGURE 1. Insect wing motion: (a) Wing path described by looking at a particular section of the wing (in red) with the dot representing the leading edge; (b) Tracking of this wing section during up and downstrokes demonstrating their translational motion and showing slope reversal due to pronation and supination interpreted as rotational motion; (c) trend in evolution of flapping and twisting in quadrature over time [5, 6]

have demonstrated that aerodynamic performance decreases with greater flexibility at low and medium angles of attack. Furthermore, the use of resonant mechanisms has also been the subject of much discussion between studies highlighting the use of the natural frequency of wings [13, 14] that yields excellent performance with low power consumption, and those demonstrating that insects have a wingbeat that is different from the resonance frequencies of the wings [7, 15], as the resonance mechanism depends on other body parts such as the thorax [16].

There seems to be no one key to insect flight and a question naturally rises: would it be possible to couple the bending and twisting resonant modes to reproduce insect wing kinematics and generate lift ? Historically, the concept of mode coupling has already been used in the fields of optics, photonics, and chemistry [17, 18], as well as in microelectromechanical systems (MEMS), to increase the sensitivity of vibrational gyroscopes [19, 20]. In music, instrument structures are also designed to tune mode frequencies non-linearly to produce complex sounds [21–23]. However, as far as we know, mechanical vibration modes are generally shifted away from the natural frequency to avoid destructive interactions with a system and are rarely used to perform a specific mechanism. Therefore, part of the challenge in this paper was to apply the concept of coupling modes in the case of a nano air vehicle (NAV) constituted of flexible artificial wings to reproduce insect wing kinematics and generate lift.

The paper is organized as follows. Section 1 recalls the flight mechanisms currently used by bioinspired Nano Air Vehicles [24, 25] and then underlines different coupling approaches. Section 2 presents the results of a systematic parametric analysis in order to conceive optimal prototype artificial wings. In Section 3, we present the experimental setup and in Section 4 we offer some concluding remarks regarding the experimental results that demonstrate the effectiveness of the coupling concept.

2 Flight mechanisms and wings kinematics

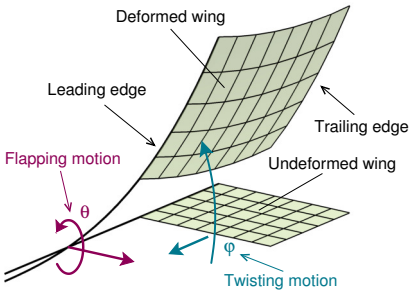

FIGURE 2. Drawing of a two degree of freedom flexible wing

In this study, we consider a fully flexible wing (Fig. 2), whose kinematics are defined by the combination of two elementary motions: a flapping motion, described by an angle θ, and a twisting motion, described by an angle φ.

2.1 Passive resonant twisting of the wing

In general, artificial wings of micro and nano air vehicles consist of an articulated rigid leading edge attached to the thorax and a flexible membrane. To produce an appropriate wing slope and lift off [26], the most common mechanism is to impose a large flapping motion on the rigid leading edge and to exploit the passive twisting of the wing. In this case, the displacement of the leading edge during flapping is imposed but twisting has a single degree of freedom (Fig. 3). The system behavior can then be written in the following differential form:

$$\ddot{\varphi} + 2\xi\omega_0(\dot{\varphi} - \dot{\theta}) + \omega_0^2(\varphi - \theta) = 0, \qquad (1)$$

with the imposed leading edge flapping motion $\theta(t) = \theta_0 \cos \Omega t$, where ξ, ω_0, θ_0 and Ω represent the damping factor, the natural frequency of the system, the amplitude of excitation, and the frequency of excitation, respectively. The flapping motion can be written $\varphi(t) = \varphi_0 \cos(\Omega t + \alpha)$; the amplitude φ_0 and the phase α of the twisting with respect to the imposed flapping are shown in Fig. 3 as functions of the excitation frequency and the damping

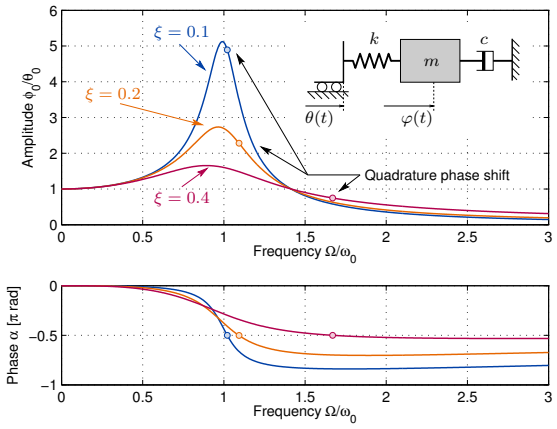

FIGURE 3. Frequency response of a single degree of freedom mass-spring-dashpot system with an imposed base motion. Amplitude and phase of the mass displacement φ with respect to the imposed motion θ.

ratio. The dashpot was placed between the mass and the ground to model aeroelastic damping.

Contrary to the amplitude, the oscillatory response of this system reveals that the phase shift between the twisting motion of the wing and the flapping motion of the leading edge is strongly dependent on the damping factor. Hence, if phase quadrature is obtained at the natural frequency ω_0 without damping, this phase quadrature shifts towards higher frequencies when the damping factor increases. As with insects, a maximum lift force can be achieved when flapping and twisting are in phase quadrature. The excitation frequency can thus be chosen in order to trigger the optimal phase shift and in general, the natural wing frequency is not used.

Based on this statement, this explains and highlights why some authors in the literature [26] claim that the maximum lift force is not found at resonance but in quadrature.

2.2 Proposed concept

The new concept proposed in this paper was to design a flexible wing such that the leading edge displacement and the twisting are both induced by the dynamic resonant behavior of the structure, with the right coupling to produce phase quadrature. To obtain such specific kinematics, the proposed solution was (1) to consider two natural vibration modes of which the deformed shapes are close to a bending motion for the first one and close to a twisting motion for the second one, and (2) to design the elastic properties of the wing structure so that their natural frequencies are close to each other.

To illustrate this concept, let us consider a reduced order dynamical model of the flexible wing, truncated to only two natural modes. The displacement of a point x of the wing is written as a

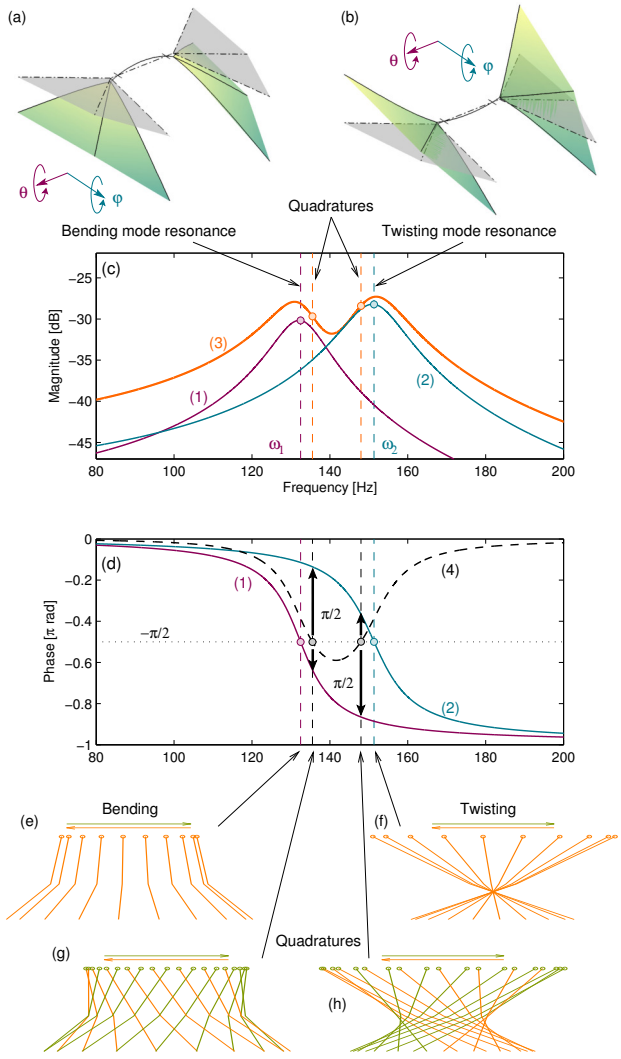

FIGURE 4. Theoretical prototype mode shapes: (a) bending; (b) twisting. Amplitude and phase of the theoretical frequency responses of the prototype: (c) amplitude of (1) bending and (2) twisting modal coordinates; (3) amplitude of their combination; (d) bending (1) and twisting phases (2) and their difference (4). Wing tip motion tracking seen from one side: (e) bending resonance, (f) twisting resonance, (g,h) quadrature motion

function of space and time:

$$u(x,t) = \Phi_1(x)q_1(t) + \Phi_2(x)q_2(t) \tag{2}$$

with $q_1(t)$ and $q_2(t)$ being the modal coordinates and $\Phi_1(x)$ and $\Phi_2(x)$ the modal shapes of the two modes retained (bending and twisting, respectively). These two mode shapes are illustrated in Fig. 4(a,b). More precisely, the bending mode shape $\Phi_1(x)$ cor-

responds to a motion with θ and φ in phase whereas the twisting mode shape $\Phi_2(x)$ results in phase opposition between θ and φ.

According to classical vibration theory [27], the two modal coordinates $q_1(t)$ and $q_2(t)$ satisfy the following differential equation:

$$\ddot{q}_i(t) + 2\xi_i\omega_i\dot{q}_i(t) + \omega_i^2 q_i(t) = F_i\cos\Omega t, \quad i = 1,2, \qquad (3)$$

where ξ_1 and ξ_2 are the damping factors of each mode, ω_1 and ω_2 are their natural frequencies, F_1 and F_2 are the modal forcing terms, and Ω is the harmonic excitation frequency. These modal coordinates can be written $q_1(t) = a_1\cos(\Omega t + \alpha_1)$ and $q_2(t) = a_2\cos(\Omega t + \alpha_2)$ in the steady state. If $\xi_i < \sqrt{2}$, the response is resonant, as shown in Figs. 4(c,d) ((1) for bending mode and (2) for twisting mode). The frequency response of the wing is also shown (line (3)) and results from the modal combination of Eq. (2).

Amplitudes a_1 and a_2 are maximum for $\Omega \simeq \omega_1, \omega_2$, where the phases α_1, α_2 cross the $\pi/2$ value. As shown in Fig. 4(d), there are two other frequencies between the resonance frequencies for which the phase difference is $\alpha_2 - \alpha_1 = \pi/2$ and corresponds to kinematics with the bending and twisting motion in quadrature. To illustrate these particular kinematics, wing tip motion tracking, seen from the side, is shown in Figs. 4(e,f,g,h). For an excitation frequency close to the two bending and twisting resonances ($\Omega \simeq \omega_1, \omega_2$), the wing motion is synchronous and corresponds to one of the oscillatory mode shapes. At the two quadrature frequencies, it is clear from Figs. 4(g,h) that the bending and twisting mode shapes are both activated in quadrature, and that the resulting wing motion is similar to that of an insect wing shown in Fig. 1(b).

Consequently, the proposed concept has two remarkable properties. First, it results in the right coupling of the bending and twisting motion to recreate the movement of an insect wing. Second, since the two quadrature actuation frequencies are close to the bending and twisting resonances, the wings respond with a large amplitude suitable to maximize the lift force.

2.3 Aeroelastic modeling

In order to estimate the evolution in lift force as a function of frequency using a simple dimensional analysis, the force applied by a fluid on an immersed rigid body obeys the following expression:

$$F = \frac{1}{2}C_d(Re,\Gamma)\rho S V^2 \qquad (4)$$

where S is the surface of the wing, ρ is the fluid density, V is the fluid velocity field, and the drag coefficient C_d is a function of the Reynolds number Re and the geometry Γ of the immersed body. This is the so-called steady fluid force because the fluid velocity field around the body is time independent. If the speed of the body changes slowly enough over time (the time variations of $V(t)$ are small with respect to V), the previous formula still holds as $F(t) = \frac{1}{2}C_d(Re,\Gamma)\rho S V^2(t)$. This is known as the quasi-steady force.

The flapping wing nanodrone developed in this study has a wingspan of 2.2 cm and a flapping frequency of 190 Hz. The wings vibrate at a velocity in the order of 190 cm/s. Since the kinematic viscosity of air is around $10^{-5}m^2/s$, these data yield a Reynolds number of $Re = 1900$, i.e. the fluid is in transition to turbulence.

Studies carried out [28] on flat plates at transitional Reynolds numbers, as well as with high Reynolds numbers [29], have shown that a very good correlation could be obtained if we consider the expression (4) containing the squared velocity. In addition, both studies considered an added-mass term for a better correlation with the experimental results obtained with oscillating plates. The complete model is called the Morrison equation:

$$F = \frac{1}{2}C_d\rho S V^2 + C_m\rho Vol\frac{dV}{dt} \qquad (5)$$

where Vol is the bodys volume and C_m is the so-called inertia coefficient, which once again depends on the Reynolds number Re, the geometry, and its trajectory. For example, its value is 0.5 for an accelerating sphere in potential flow. The thoroughly studied added-mass effect [30] appears due to the inertia of the fluid. Its associated force is thus proportional to the time derivative of the bodys speed. This effect clearly cannot be taken into account by the classical steady formula (4).

Those added-mass forces only contribute for a virtual change in the bodys mass. Since the resonant oscillatory motion of the body will be considered in the following, those added-mass, proportional to the acceleration $\frac{dV}{dt}$ of the body, contribute only to a small change in the natural frequency of the body. Consequently, we will suppose that the corrected natural frequency has been taken into account in the development of the structural model of the nanodrone, and only the steady component (the first term of Eq. 3) of the fluid force will be considered from now on. Moreover, since this study is for hovering, the only fluid velocity present is induced by the wings' motion and the free stream one is taken as null.

As the drag coefficient C_d depends on the wing geometry, trajectory, and the Reynolds number, it seems unrealistic to aim to obtain an extremely accurate and reasonably computable drag coefficient model. Our purpose here was to obtain an aerodynamic model which can return values within the correct order of magnitude; the value will then be set to $C_d = 1$ (its lower and upper bounds known to be respectively 0.5 and 10).

It is well known that the tangential component of the force is negligible compared to the normal one in the case of flat plates

in sinusoidal motion. In our aerodynamic model, the force will also be taken as orthogonal to the wings surface.

It is known that oscillatory flow parallel to a flat plate produces a purely tangential force without any normal component, regardless of the Reynolds number. Therefore, our expression will have to be reduced when V is orthogonal to the normal surface n.

Since the wings are deformable and can thus change shape as a function of time, neither the velocity field nor the normal vector is uniform on the wing surface. However, the fluid problem is mathematically a boundary value problem, i.e. the value of any magnitude at a single point will, in general, depend on the value in the whole fluid domain, typically by means of a volume integral. In linear theory, this influence or dependency is determined by mapping using a Greens function. In this study, we will assume that this influence will decay fast enough from any two points on the wing. We can, therefore, consider that local aerodynamic effects are of first order and we can estimate the local force by only evaluating local variables.

By the above consideration, the force model that will be used in our calculations is:

$$F = -\frac{1}{2}\rho \iint_{Wing} |V|(V.n)ndS \tag{6}$$

where the local force per unit surface area (the integrand) opposes the wings speed direction and the velocity field V now depends on a local point on the wing surface.

From this model, the calculations are then processed by numerical integration of the local aerodynamic forces applied to the wing kinematics obtained with the modal modeling described previously in equation (3). The lift force generated by the different wing kinematics over the working frequency range can then be computed.

In Fig 5, the bending amplitude of the wing tip (in green) has been plotted against the forcing frequency and the associated mean lift force (in blue); the mean was calculated over a flapping period. We can observe two local maxima for the lift which are very close to the quadrature frequencies at 134.8 Hz and 146.7 Hz (highlighted by vertical red lines). The left peak is located between the resonance frequency (maximal amplitude) and the quadrature frequency (optimal kinematics, i.e. the closest from insects' ones). The other local maximum is located exactly at the second quadrature frequency, as its related amplitude is relatively constant in its neighborhood. These important results are in agreement with those obtained by [31].

Although high bending amplitudes are necessary to generate lift, they are not sufficient. The second lift maximum is located at the local minimum of the bending amplitude, which is a quadrature frequency. This proves that good coordination between the

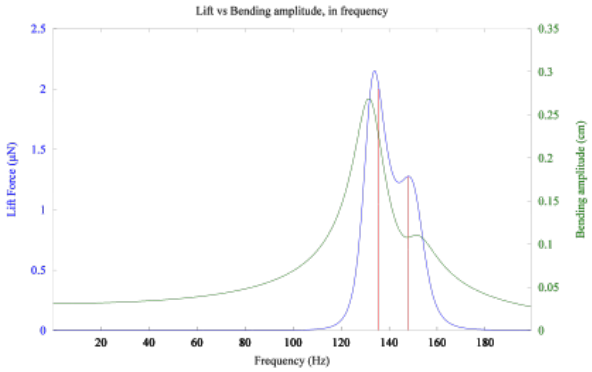

FIGURE 5. Bending amplitude (green) vs. mean lift force (blue) over a period of movement, plotted against the applied forcing frequency

twisting and bending motions is the real driving force behind lift generation.

The reason behind this is that flapping movement alone does not generate lift; twisting is also involved, and the twisting amplitude of the second quadrature peak is much higher than the first one.

A smaller lift force is associated with the second quadrature frequency since the amplitudes of the first are much larger.

3 Prototype design

3.1 Structure and manufacturing

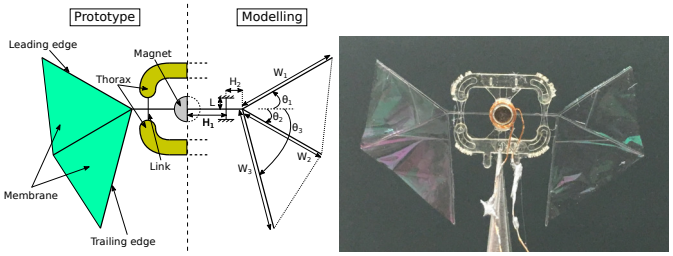

FIGURE 6. NAV prototype with SU-8 skeleton, Parylene C wings and electromagnetic actuator with a total mass of 22 mg

The prototype was fabricated with dedicated MEMS technologies to allow highly accurate design tolerance. It is composed of a 3D skeleton made from multiple layers of photo-resist SU-8, with thicknesses ranging between 40 μm and 150 μm (Fig. 6). The wing membranes, composed of a thin film 400 nm thick of Parylene C, were deposited on the skeleton veins resulting in wings 22 mm in length. All the details can be found in [32]

Wing actuation relies on the vertical electromagnetic force applied to the magnet when a sinusoidal current flows through the coil. To drive both wings simultaneously, the prototype was fitted with a single electromagnetic actuator placed in the middle of the thorax. The latter has the advantage of being easy to manufacture and integrate into our prototype, having a simple geometry, fast response speed, and high bandwidth, and more particularly the possibility of tuning a wide range of frequencies. The electromagnetic actuator comprises a magnet stuck to the tergum which is slipped into a copper coil fixed to the thorax, as presented in Fig. 6. A cylindrical neodymium iron boron magnet Ni-N48 (HKCM) 0.5 mm thick, 1.5 mm in diameter, and weighing 6 mg was selected. The coil was made in-house using 80 μm diameter enameled copper wire; the number of turns was 20.

The total weight of the prototype is 22 mg, which means it is currently the smallest and lightest flexible-wing NAV.

3.2 Wing geometry

The flexible structure of the wing was modeled using Euler-Bernoulli beam deformation in a vacuum. The structural effect of the wing membranes was neglected, as their thickness is very small compared to the veins. These assumptions are justified since our primary goal was to design the wing geometry such that the natural frequencies of the bending and twisting vibration modes were close. To this end, a parametric analysis of the wing vein geometry proposed in Fig. 6 was performed. Among the constraints, the geometry of the thorax was imposed and the resonant modes had to be between 100 Hz and 200 Hz using the photoresist polymer SU-8, a material considered as equivalent to that of natural insect wings [33–35]. Evidently, the key issue of this analysis was to bring the frequencies of two natural modes closer, as explained in the previous section.

To this end, an optimization of the geometrical parameters $(\theta_i, W_i, H_i \ldots)$ of the wing vein geometry of Fig. 6, based on a theoretical modal analysis, was performed. The main constraints were to bring the frequencies of the two natural modes as close as possible to each other and lying between 100 Hz and 200 Hz. The geometry of the thorax was imposed.

According to this parametric study, an optimal wing vein configuration was obtained, as illustrated in Fig. 6. Its frequency response is shown in Fig. 4, with damping ratios $\xi_1 = \xi_2 = 5\%$ chosen in Eq. (3) to fit the experiments. The viscous damping included here was used to take into account the damping effect of the aeroelastic forces. Even though multiple solutions exist, the one proposed here appears to be satisfactory since the two coupled modes are only 20 Hz apart, with the bending mode occurring at 130.2 Hz and the twisting mode at 151.4 Hz for the wings created. This now means that quadrature coupling of these modes is possible just by tuning the excitation frequency. The use of two resonant modes yields two solutions to obtain the quadrature shift between each resonance. The first one is at 134.8 Hz and the second one is at 146.7 Hz, very close to the bending and twisting resonances, thus resulting in a relatively large amplitude of wing motion.

Figs. 4(e,f,g,h) depict the simulated wing chord motion for the bending mode at 130.2 Hz, the twisting mode at 151.4 Hz, and the quadrature motions at 134.8 and 146.7 Hz, respectively. It is clear that the wing slope during each stroke is almost null for the bending mode, while during tracking of the twisting mode the slope is not conserved during the stroke. For these bending and twisting modes, no lift can be generated. As expected, coupling these modes with a quadrature phase shift allows insect wing kinematics to be reproduced (Fig. 1) since the maximum slope between the leading and trailing edge occurs when the wing is halfway between the upstroke and the downstroke, with slope reversal at the end of each stroke.

4 Experimental setup

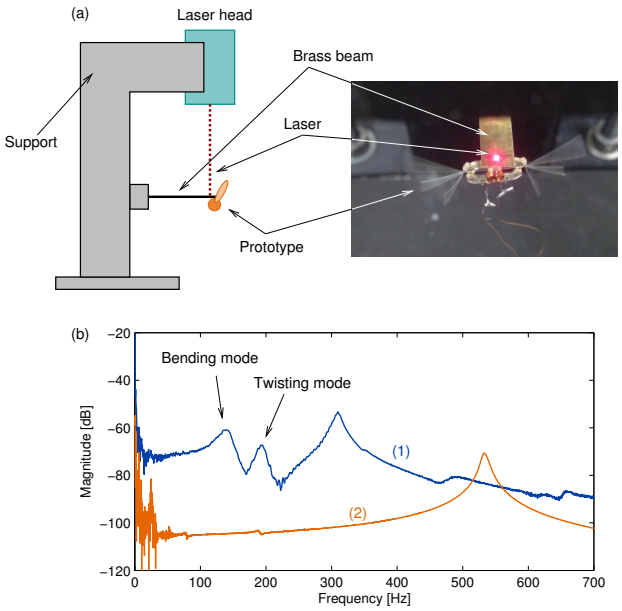

FIGURE 7. (a) Experimental setup for measuring lift force (b) Frequency response measurement using PSV400 laser vibrometer; (1) Frequency Response Function (FRF) of the prototype taken at the magnet under normal operation (prototype magnet driven by sine sweep); (2) FRF of the tip of the brass beam with the non-actuated prototype glued to it and directly driven by an additional magnet coil system.

In order to estimate both the kinematics and the lift force generated by the prototype during wing actuation, a specific test bench with different measuring devices for each of the various measurements required was developed as shown in Fig. 7(a). It

comprises a brass cantilever beam to which the prototype was glued, the goal being to correlate the cantilever displacement with the NAV aerodynamic force.

A Polytec PSV400 scanning laser vibrometer was used to measure the velocity at several points on the skeleton of the prototype during a sine sweep input excitation. More precisely, the frequency spectrum of the velocity signal was divided by that of the input electric current in the coil to obtain the Frequency Response Function (FRF) of the corresponding point. An example is shown in Fig. 7(b), line (1).

The laser vibrometer was also used to measure the passive response of the brass beam to identify its lowest resonance frequency (Fig. 7(b), line (2)). It was then verified that it was greater than twice those of the prototype bending and twisting resonance frequencies, which lie between 150 Hz and 250 Hz. This condition was necessary to ensure that the cantilever displacement could be used to determine the lift force generated by a simple proportionality relation independent of the actuation frequency.

The linear relation between the force applied to the cantilever tip and its jib was evaluated at 180 μN/μm using both an FT-S1000 microforce sensing probe and an FT-1000 mechanical probe from Femto-Tools. The lift force was then obtained during wing prototype actuation by measuring the displacement of the cantilever using a CCD laser (LK-G32 Keyence) that can measure displacements in the order of 0.1 μm, so a minimum force of approximately 20 μN could be measured.

5 Results analysis and discussion

Using the experimental setup described in the previous section, we tested the performance of the optimal wing configuration presented in Fig. 6. The percentage was determined by the parametric analysis. Firstly, the FRFs at several points on the prototype skeleton were measured using the PSV400 scanning laser vibrometer. These values were then used to reconstruct the deflection shape of the prototype at several actuation frequencies. The FRF at the magnet is depicted in Figs. 7(b) and 8(c) and shows two resonances at 140 Hz and 195 Hz. The corresponding deflection shapes are presented in Figs. 8(a,b) and they are clearly associated with the bending and twisting modes. The experimental results are impressively close to those obtained in simulation. First, the experimental mode shapes were similar to the ones predicted. Then, a minimal difference in frequency of 60 Hz was successfully obtained between the bending and twisting modes. Obviously, the theoretical difference was smaller (about 20 Hz), which can be explained by the aeroelastic effects neglected in the model. These effects are responsible for damping and added mass effects that change the resonance frequencies.

In a second step, the lift force was measured in the steady state at several frequencies around the bending and twisting resonance frequencies using the proposed test bench. Fig. 8(d)

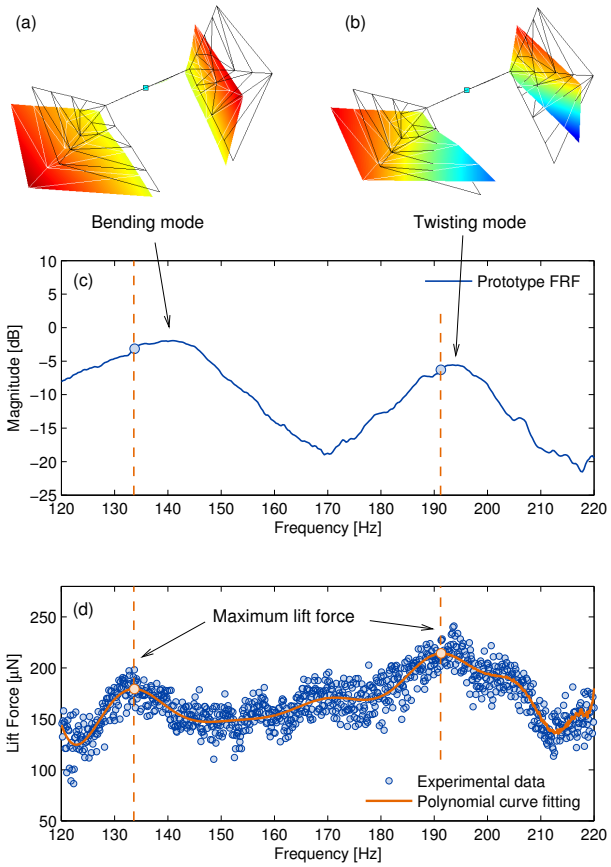

FIGURE 8. Experimental deflection shapes at resonance: (a) bending mode; (b) twisting mode; (c) Frequency response function (FRF) of the prototype taken at the magnet and zoomed over the frequency range of interest; (d) Average lift force over one period for several excitation frequencies. Polynomial curve fit.

shows the lift force averaged out over a period of motion and a polynomial curve fit. Good precision was obtained for such levels of force since an uncertainty of approximately 10% was observed. Furthermore, two maximum values of the averaged lift force were observed near the bending and twisting modes, at 133.5 Hz and 190.8 Hz, respectively. Obviously, these maximum values correspond to the phase quadrature frequencies in accordance with the theoretical results (Fig. 4(d)) and aeroelastic modeling (Fig. 5), and as shown by the high-speed camera measurements below. Moreover, the second value near the twisting mode, 220 μN, was sufficient to overcome the prototype weight, equivalent to 200 μN. In addition, the main goal of this study was to use the quadrature coupling of two resonant modes to produce lift, and this was definitely achieved and validated.

To supplement this discussion, Fig. 9 presents the instantaneous force measured as a function of time as well as the associ-

ated frequency spectrum for the second quadrature frequency. In addition to the continuous component, two frequency peaks can be distinguished: one at the actuation frequency of 190.8 Hz corresponding to the drag force, and the other at the second harmonics frequency of 381.6 Hz associated with the lift force, as frequency doubling is related to slope variation during the strokes. As shown by [4, 36], the averaged force obtained corresponds to the effective lift force.

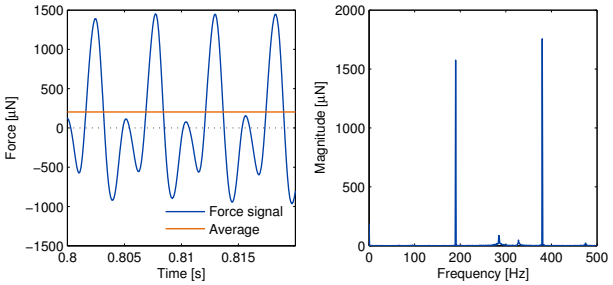

FIGURE 9. Lift force versus time at the second quadrature actuation frequency (190.8Hz) and related frequency spectrum.

Finally, the observation and tracking of the wing chord motion using a high-speed camera (Phantom V7.4 from Vision) is illustrated in Fig. 10. From this figure, it can be concluded once again that the experimental motion presents the expected wing kinematics with the leading and trailing edges in quadrature. This underlines the interest of using coupled resonant modes in quadrature to generate lift.

6 Conclusion

In this paper, a new mechanism to generate sufficient lift to overcome the weight of a flexible wing NAV was presented. This mechanism is based on the coupling in quadrature of two natural bending and twisting vibratory modes of the wings. As mentioned, the first key issue of this work was to bring the frequency of the two modes closer together in order to reproduce insect wing kinematics. The analytical parametric modeling solved this issue and provided an optimal geometrical wing configuration. Furthermore, aerodynamic modeling validated the concept by predicting the maximum lift generated at the quadrature frequencies. Experimental studies were then conducted on this configuration and the kinematics and the evolution in lift in relation to the frequency were in excellent agreement with the theoretical predictions. Finally, it was demonstrated that our prototype was able to generate a lift force of 110% in relation to its weight, which validated this new concept.

Future work must now focus not only on wing configuration but also on the actuation and transmission parts in order to increase the bending amplitude and enable take off. To achieve this goal, a multi-criteria analysis needs to be performed to optimize a cost function according to the take-off objective. The criteria could be based on structural parameters such as wing and thorax geometries, mode frequencies, and mode excitability, as well as aerodynamic parameters such as wing membrane surface and force distribution. Furthermore, although the predicted lift force is in good agreement with measured one in term of evolution with frequency it is still a qualitative model and will need to be improved by taking account of large displacement and by calibrating the aerodynamic coefficients. The lift force test bench could also be improved, with a second sensor to identify the best inclination angle of the prototype.

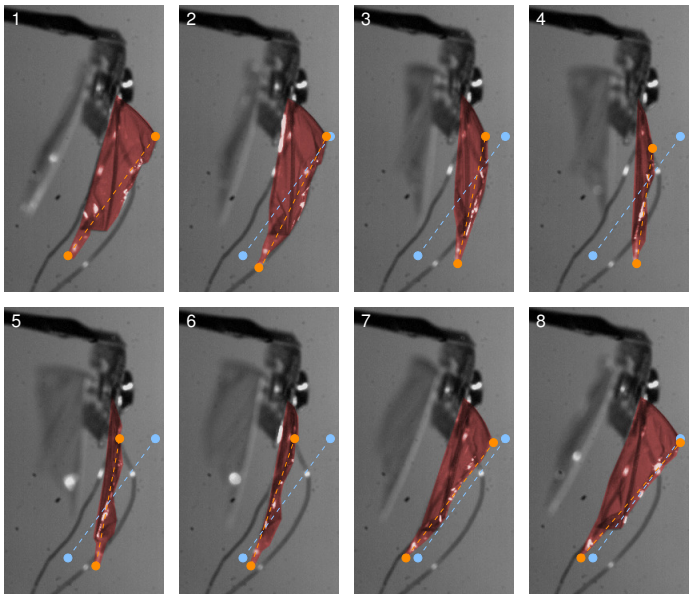

FIGURE 10. Several frames captured using a high-speed camera at the second quadrature actuation frequency (190.8Hz). Blue dashed line: initial chord position; Orange dashed line: current chord position. Slope inversion occurs around frame 4.

ACKNOWLEDGMENT

This work was supported by ANR-ASTRID CLEAR-Flight (ANR-13-ASTR-0012), the RENATECH program, the Direction Generale de l'Armement, and the Haut-de-France Region.

REFERENCES

[1] Srygley, R., and Thomas, A., 2002. "Unconventionnal lift generating mechanism in free flying butterflies". *Nature,* ***420***, pp. 660–664.

[2] Wootton, R., 1991. "The functional morphology of the

wings of odonata". *Advances in odonatology,* ***5***(1), pp. 153–169.

[3] Wootton, R., 1999. "How flies fly". *Nature,* ***400***(6740), July, pp. 112–3.

[4] Dickinson, M., 1999. "Wing Rotation and the Aerodynamic Basis of Insect Flight". *Science,* ***284***(5422), June, pp. 1954–1960.

[5] Fry, S. N., Sayaman, R., and Dickinson, M. H., 2003. "The aerodynamics of free-flight maneuvers in drosophila". *Science,* ***300***, pp. 495–498.

[6] Seshadri, P., Benedict, M., and Chopra, I., 2012. "A novel mechanism for emulating insect wing kinematics". *Bioinspir. Biomim.,* ***7***, p. 036017.

[7] Chen, J.-S., Chen, J.-Y., and Chou, Y.-F., 2008. "On the natural frequencies and mode shapes of dragonfly wings". *Journal of Sound and Vibration,* ***313***(3-5), June, pp. 643–654.

[8] Ennos, 1988. "The importance of torsion in the design of insect wings". *Journal of experimental biology,* ***140***(1), November, pp. 137–160.

[9] Ennos, 1988. "The inertial cause of wing rotation in Diptera". *Journal of experimental biology,* ***140***(1), November, pp. 161–169.

[10] Mountcastle, A., and Daniel, 2009. "Aerodynamic and functional consequences of wing compliance". *T.L. Experiments in fluids,* ***46***, May, p. 873.

[11] Young, J., Walker, S., Bomphrey, R., Taylor, G., and Thomas, A., 2009. "Details of insect wing design and deformation enhance aerodynamic function and flight efficiency". *Science,* ***325***(5947), September, pp. 1549–52.

[12] Zhao, L., Huang, Q., Deng, X., and Sane, S., 2010. "Aerodynamic effects of flexibility in flapping wings". *Journal of the royal society Interface,* ***7***, pp. 485–497.

[13] Michelin, S., and Llewellyn Smith, S., 2009. "Resonance and propulsion performance of a heaving flexible wing". *Physics of Fluids,* ***21***(7), July.

[14] Masoud, H., and Alexeev, A., 2010. "Resonance of flexible flapping wings at low Reynolds number". *Physical Review E - Statistical, Nonlinear, and Soft Matter Physics,* ***81***(5), May.

[15] Ha, N., Truong, Q., Goo, N., and Park, H., 2013. "Relationship between wingbeat frequency and resonant frequency of the wing in insects.". *Bioinspiration & biomimetics,* ***8***(4), December.

[16] Hrncir, M., Gravel, A.-I., Schorkopf, D., Schmidt, V., Zucchi, R., and Barth, F., 2008. "Thoracic vibrations in stingless bees (Melipona seminigra): resonances of the thorax influence vibrations associated with flight but not those associated with sound production.". *The Journal of experimental biology,* ***211***(Pt 5), March, pp. 678–85.

[17] McCutcheon, M., Young, J., Rieger, G., Dalacu, D., Frederick, S., Poole, P., Aers, G., and Williams, R., 2006. "Second-Order Nonlinear Mixing of Two Modes in a Planar Photonic Crystal Microcavity". *Physics,* ***2***, January.

[18] O.V. Misochko and E.I. Rasi-Iba and E.Y. Sherman and V.B. Timofeev , 1990. "On the mixing of vibrational modes in high-t superconductors". *Physics Reports (Physics Letter),* ***6***(194), November, pp. 387–395.

[19] Zaman, M., Sharma, A., and Ayazi, F., 2006. "High performance matched-mode tuning fork gyroscope". *IEEE MEMS*, January, pp. 66–69.

[20] Leland, R., 2003. "Adaptive Mode Tuning for Vibrational Gyroscopes". *IEEE Transactions on control systems technology,* ***11***(2), March, pp. 242–247.

[21] Monteil, M., Thomas, O., and Touzé, C., 2015. "Identification of mode couplings in nonlinear vibrations of the steelpan". *Applied Acoustics,* ***89***(2015), March, pp. 1–15.

[22] Rossing, T., and Perrin, R., 1987. "Vibrations of bells". *Applied Acoustics,* ***20***(1), pp. 41–70.

[23] Fletcher, N., 1993. "Tuning a pentangle : A new musical vibrating element". *Applied Acoustics,* ***39***(3), pp. 145–163.

[24] Wood, R., 2008. "The First Takeoff of a Biologically Inspired At-Scale Robotic Insect". *IEEE Transactions on Robotics,* ***24***(2), April, pp. 341–347.

[25] Raney, D., and Slominski, E., 2003. "Mechanization and Control Concepts for Biologically Inspired Micro Aerial Vehicles". *AIAA,* ***5345***, August.

[26] Ramananarivo, S., Godoy-Diana, R., and Thiria, B., 2011. "Rather than resonance, flapping wing flyers may play on aerodynamics to improve performance". *Proceedings of the National Academy of Sciences of the United States of America,* ***108***(15), pp. 5964–5969.

[27] Géradin, M., and Rixen, D., 2015. *Mechanical Vibrations: Theory and Applications to Structural Dynamics*, 3rd ed. J. Wiley & Sons.

[28] Shih, C. C., and Buchanan, H. J., 1971. "The drag on oscillating flat plates in liquids at low reynolds numbers". *Journal of Fluid Mechanics,* ***48(2)***, pp. 229–239.

[29] Keulegan, G. H., and Carpenter, L. H., 1958. "Forces on cylinders and plates in an oscillating fluid". *Journal of Research of the National Bureau of Standards,* ***60(5)***, pp. 423–440.

[30] Lamb, H., 1932. *Hydrodynamics*, 1st ed. Cambridge university press.

[31] Frampton, K. D., Goldfarb, M., Monopoli, D., and Cveticanin, D., 2000. "Passive aeroelastic tailoring for optimal flapping wings". *Proceeding of the Fixed, Flapping and Rotary Wing Vehicles at Very Low Reynolds Numbers*, pp. 26–33.

[32] Bao, X., Bontemps, A., Grondel, S., and Cattan, E., 2011. "Design and fabrication of insect-inspired composite wings for MAV application using MEMS technology". *Journal of Micromechanics and Microengineering,* ***21***(12), November.

[33] Bontemps, A., Vanneste, T., Paquet, J.-B., Dietsch, T., Grondel, S., and Cattan, E., 2013. "Design and performance of an insect-inspired nano air vehicle". *Smart Materials and Structures,* ***22***(1), January.

[34] Dargent, T., Bao, X., Grondel, S., Brun, G. L., Paquet, J.-B., Soyer, C., and Cattan, E., 2009. "Micromachining of an SU-8 flapping-wing flying micro-electro-mechanical system". *Journal of Micromechanics and Microengineering,* ***19***(8), July.

[35] Bao, X., Dargent, T., Grondel, S., Paquet, J., and Cattan, E., 2011. "Improved micromachining of all SU-8 3D structures for a biologically-inspired flying robot". *Microelectronic Engineering,* ***88***(8), August, pp. 2218–2224.

[36] Lehmann, F.-O., Sane, S., and Dickinson, M., 2005. "The aerodynamic effects of wing-wing interaction in flapping insect wings". *The Journal of experimental biology,* ***208***(16), pp. 3075–3092.